Clinical Evaluation of (4S)-4-(3-[^{18}F]Fluoropropyl)-L-glutamate (^{18}F-FSPG) for PET/CT Imaging in Patients with Newly Diagnosed and Recurrent Prostate Cancer

Sonya Youngju Park[1,2], Sae Jung Na[1,3], Meena Kumar[2], Camila Mosci[2], Mirwais Wardak[2], Norman Koglin[4], Santiago Bullich[5], Andre Mueller[4], Mathias Berndt[4], Andrew W. Stephens[4], Yong Mee Cho[6], Hanjong Ahn[7], Sun Young Chae[3], Hye Ok Kim[3,8], Dae Hyuk Moon[3], Sanjiv S. Gambhir[2,9], and Erik S. Mittra[2,10]

ABSTRACT

Purpose: (4S)-4-(3-[^{18}F]Fluoropropyl)-*L*-glutamic acid (^{18}F-FSPG) is a radiopharmaceutical for PET imaging of system x_C^- activity, which can be upregulated in prostate cancer. We present data on the first evaluation of patients with newly diagnosed or recurrent prostate cancer with this radiopharmaceutical.

Experimental Design: Ten patients with primary and 10 patients with recurrent prostate cancer were enrolled in this prospective multicenter study. After injection of 300 MBq of ^{18}F-FSPG, three whole-body PET/CT scans were obtained. Visual analysis was compared with step-section histopathology when available as well as other imaging studies and clinical outcomes. Metabolic parameters were measured semiquantitatively. Expression levels of xCT and CD44 were evaluated by IHC for patients with available tissue samples.

Results: ^{18}F-FSPG PET showed high tumor-to-background ratios with a relatively high tumor detection rate on a per-patient (89%) and per-lobe (87%) basis. The sensitivity was slightly higher with imaging at 105 minutes in comparison with 60 minutes. The maximum standardized uptake values (SUV_{max}) for cancer was significantly higher than both normal ($P < 0.005$) and benign pathology ($P = 0.011$), while there was no significant difference between normal and benign pathology ($P = 0.120$). In the setting of recurrence, agreement with standard imaging was demonstrated in 7 of 9 patients (78%) and 13 of 18 lesions (72%), and revealed true local recurrence in a discordant case. ^{18}F-FSPG accumulation showed moderate correlation with CD44 expression.

Conclusions: ^{18}F-FSPG is a promising tumor imaging agent for PET that seems to have favorable biodistribution and high cancer detection rate in patients with prostate cancer. Further studies are warranted to determine the diagnostic value for both initial staging and recurrence, and how it compares with other investigational radiotracers and conventional imaging modalities.

Introduction

Prostate cancer is the most common malignancy in men (1) and the second leading cause of cancer-related death in American men, behind only lung cancer (2). Although those with localized disease receive treatment with curative intent, approximately 35% of patients with prostate cancer will experience biochemical recurrence within a decade of initial therapy (3). Disease evolution to an eventual castrate-resistant metastatic state carries a significantly worse outcome with poor survival.

Serum PSA is the most widely used biomarker for prostate cancer detection. However, establishing the appropriate cut-off value for diagnosis has been a challenge because it is also expressed in hyperplastic cells, especially benign prostatic hyperplasia (BPH). Meanwhile, biopsy remains the only definitive way to confirm prostate cancer. This role is more limited in the case of recurrence because of its unreliable negative predictive value. Accurate noninvasive tumor imaging for biopsy guidance would therefore have great impact on early detection, risk stratification, and disease monitoring.

Conventional imaging modalities, including CT and radionuclide bone scan, each have their strengths and limitations, but performance has generally been poor. Solitary or equivocal abnormalities may often require correlation with MRI or bone biopsy. Advanced technologies such as multiparametric MRI and nuclear imaging with PET could improve diagnostic accuracy (4–6).

Several PET radiotracers are currently being used and investigated for the detection and characterization of prostate cancer. ^{18}F-FDG is widely used for tumor imaging, but it is inadequate due to the relatively weak glucose metabolism in small, slow-growing prostate cancer cells

[1]Department of Radiology, College of Medicine, The Catholic University of Korea, Seocho-gu, Seoul, Republic of Korea (South). [2]Molecular Imaging Program at Stanford (MIPS), Department of Radiology, Stanford University, Stanford, California. [3]Department of Nuclear Medicine, Asan Medical Center, University of Ulsan College of Medicine, Songpa-gu, Seoul, Republic of Korea (South). [4]Bayer Pharma AG, Berlin, Germany. [5]Life Molecular Imaging GmbH, Berlin, Germany. [6]Department of Pathology, Asan Medical Center, University of Ulsan College of Medicine, Songpa-gu, Seoul, Republic of Korea (South). [7]Department of Urology, Asan Medical Center, University of Ulsan College of Medicine, Songpa-gu, Seoul, Republic of Korea (South). [8]Department of Nuclear Medicine, Ewha Woman's University College of Medicine, Seodaemun-gu, Seoul, Republic of Korea (South). [9]Department of Bioengineering, Department of Materials Science & Engineering, Stanford Bio-X Program, Stanford University, Stanford, California. [10]Department of Diagnostic Radiology, Oregon Health & Science University, Portland, Oregon.

S.Y. Park and S.J. Na contributed equally to this article.

Current address for N. Koglin, A. Mueller, M. Berndt, and A.W. Stephens: Life Molecular Imaging GmbH, Berlin, Germany.

Clinical Trial Identifiers: Patients were enrolled as part of NCT01186601 and NCT01103310.

Corresponding Author: Erik S. Mittra, Oregon Health & Science University School of Medicine, Portland, OR 97239. Phone: 503-494-4974; Fax: 503-494-4982; E-mail: mittra@ohsu.edu

Clin Cancer Res 2020;26:5380–7

doi: 10.1158/1078-0432.CCR-20-0644

Translational Relevance

This is the first experience of the fluorine-18–labeled glutamate derivative, (4S)-4-(3-[^{18}F]Fluoropropyl)-*L*-glutamic acid, (^{18}F-FSPG) for PET imaging of patients with primary and recurrent prostate cancer. The tracer is taken up by system x_C^-, which plays a well-documented role in cellular redox homeostasis. Results of this study provide further hints of deranged redox biology occurring also in prostate cancer, and present another potential pathway for molecular imaging and targeted therapy. The data presented in this study show ^{18}F-FSPG accumulation is demonstrated in the setting of both primary prostate cancer and biochemical recurrence. ^{18}F-FSPG uptake is also correlated to pathology and IHC for markers of system x_C^-, including xCT and CD44 expression. ^{18}F-FSPG PET/CT was able to successfully differentiate cancerous prostate lesions from normal tissue as well as benign pathologies. This promising initial study in this group of patients suggests the need for more extensive research to better understand its potential role in clinical management.

and the significant overlap with normal tissue and BPH. Robust evidence for imaging lipogenesis during cellular proliferation led to the FDA approval of ^{11}C-choline in 2013, but its diagnostic performance may depend on serum PSA level and PSA kinetics, such as PSA doubling time and PSA velocity (7). In addition, the short half-life of carbon-11 makes it impractical for widespread clinical use. Anti-1-amino-3-^{18}F-fluorocyclobutane-1-carboxylic acid (anti-^{18}F-FACBC, now known more commonly as ^{18}F-fluciclovine) has FDA approval for the identification of recurrent prostate cancer in patients with biochemical recurrence after previous treatment. It accumulates via overexpression of the amino acid transport systems. Early studies suggest that ^{18}F-fluciclovine may be advantageous over ^{11}C-choline in disease localization, although lack of specificity for differentiating between benign hyperplastic and malignant prostate lesions remains a limitation (8). Another promising target is the prostate-specific membrane antigen (PSMA), which provides a rational target for ligand receptor–based imaging and therapy (9), but is only clinically available in the United States as the indium-111–radiolabeled ProstaScint (8, 10, 11). PET imaging with the investigational ^{68}Ga-labeled agents targeting the PSMA or the gastrin-releasing peptide receptor (GRPR) is promising, but somewhat limited by the availability of ^{68}Ga generators, and although available through the compassionate use programs in Europe, they still await FDA approval in the United States (12). Both have demonstrated favorable detection rates by targeting different biologic processes, and the respective clearance pathways may also have implications for detection of abdominal and pelvic lesions (13). The development of ^{18}F-labeled PSMA-binding tracers is ongoing (14). Other approaches for molecular imaging of prostate cancer with PET are in the preclinical stages of development (15).

(4S)-4-(3-[^{18}F]fluoropropyl)-*L*-glutamic acid (^{18}F-FSPG) is an ^{18}F-labeled glutamate derivative for PET imaging. It is specifically transported via system x_C^- as demonstrated by cell competition assays and cell uptake studies in SLC7A11-knockdown cells. Excellent tumor visualization was achieved in subcutaneous animal tumor models (16). Biodistribution analysis in rodents showed rapid blood clearance via the kidneys and low background activity, providing high contrast for tumor imaging. Radiosynthesis and preclinical data of ^{18}F-hGTS13 and ^{18}F-5-fluoro-*L*-aminosuberic acid, other tracers taken up by system x_C^- and used for tumor visualization, were described recently in tumor models (17–19). Pilot clinical studies examining safety, dosimetry, and biodistribution of ^{18}F-FSPG in healthy volunteers (20, 21) and the tumor detection in various tumor entities showed promising results (22–27).

The xCT subunit of system x_C^-, which imparts substrate specificity, maintains very low basal expression and activity in most normal tissues, but is universally upregulated as cells respond to oxidative stress (28–30). CD44 is a transmembrane protein and functions as a cellular adhesion molecule. A splice variant of CD44 interacts with and stabilizes the xCT subunit and thereby promotes cystine uptake for glutathione biosynthesis to better cope with high levels of oxidative stress (31). ^{18}F-FSPG PET imaging has also been used to assess tumor redox status, and for the possible measurement of tumor antioxidant capacity and prediction of chemotherapy resistance in preclinical models (32, 33). Overexpression of xCT has been reported for other diseases possibly associated with oxidative stress such as inflammation (34, 35). In addition, prior studies of aggressive prostate cancer with high Gleason scores indicated that xCT protein expression was significantly increased and knockdown of xCT protein inhibited prostate cancer cell invasion (36). Moreover, xCT-targeted therapy has shown potential use for arresting tumor growth and/or sensitizing these CD44-expressing cancer cells, suggesting a possible approach of tying targeted therapeutics and diagnostic agents together against prostate cancer.

Given the importance of system x_C^- in cancer biology and the promising preclinical and first clinical results of ^{18}F-FSPG in previously studied tumor entities, the aims of this study were: (i) to assess the uptake and potential role of ^{18}F-FSPG PET in patients with newly diagnosed or recurrent prostate cancer, and (ii) to correlate ^{18}F-FSPG uptake with pathology and IHC of xCT and CD44 expression.

Materials and Methods

Radiopharmaceutical preparation

Radiolabeling of ^{18}F-FSPG was accomplished as described previously (22, 26). Each production batch met the criteria listed in the specification for clarity, identity, purity, radioactive concentration, specific activity, pH, bacterial endotoxin level, and sterility. The final product was formulated for intravenous injection with a drug substance per injected unit of 300 ± 30 MBq and 100 μg or less of tracer mass and a specific activity of 18.2 GBq/μmol or more.

Patients

Approval for the clinical study protocol was obtained by the Institutional Review Board at both Stanford University (Stanford, CA) and Asan Medical Center [University of Ulsan College of Medicine, Seoul, Republic of Korea (South)] as well as the Scientific Review Committee at the Stanford Cancer Institute (Stanford, CA). The U.S. and Korean Food and Drug Administrations also approved the clinical study protocol.

Twenty patients with initially diagnosed or recurrent prostate cancer were prospectively recruited for ^{18}F-FSPG PET/CT imaging. One of the patients with newly diagnosed prostate cancer did not undergo prostatectomy, and was excluded from the analysis.

PET/CT procedure

Safety parameters were assessed as described previously (26). A radioactive dose of ^{18}F-FSPG (302.5 ± 11.9 MBq; range, 282.6–321.9) with a tracer mass quantity of 2.0 ± 1.9 μg (range, 0.1–5.3 μg) was administered as a slow intravenous bolus injection over 60 seconds.

After tracer injection, the cannula and injection system were flushed with 10 mL normal saline (0.9% NaCl).

Three ^{18}F-FSPG PET/CT scans were then acquired sequentially to capture different timepoints after tracer injection. The images were obtained using a GE Discovery 600 or 690 PET/CT Scanner (GE Healthcare) or Biograph TruePoint 40 PET/CT Scanner (Siemens Medical Solutions). The first image acquisition, with a total duration of 45 minutes, was done immediately after the injection of tracer. It was performed as five sequential whole-body (vertex to mid-thigh) PET scans after obtaining one CT scan (140 kV; range, 10–85 mA) for attenuation correction and anatomic localization. Each of these five PET scans slowly increased in the number of minutes per bed position as follows: 30 seconds/bed, 30 seconds/bed, 1 minute/bed, 2 minutes/bed, and 2 minutes/bed. The second and third whole-body PET/CT scans, each with durations of approximately 30 minutes (3 minutes/bed position), were started at 60 and 105 minutes after injection, respectively. Patients were also asked to void between each scan to reduce the total radiation exposure.

Image analysis of ^{18}F-FSPG PET/CT

Visual and quantitative analysis of the ^{18}F-FSPG PET/CT images was done by consensus of five experienced nuclear medicine physicians. Visual analysis was done blinded to the clinical history, correlative imaging, or pathology results. Lesions with uptake higher than that of the background were regarded as positive. For primary prostate cancer lesions, the location of the involved segment was also described. For patients with metastases, visual analysis was done for lesions that were identified on standard imaging studies. The location and intensity of any new foci of uptake not visible on other imaging studies were also described.

Standardized uptake values (SUV) were measured on all scans (i.e., at all timepoints to track the time–activity relationship of the tracer) using the GE AW workstation. The SUV was calculated for each structure, using the formula: SUV = decay-corrected radioactivity concentration in a region of interest/(injected dose/patient's body weight).

Further analysis was performed for the delayed whole-body ^{18}F-FSPG PET/CT images at 60 and 105 minutes. The prostate was identified on the CT-registered PET images as a discrete region of uptake located inferior and slightly posterior to the urinary bladder (37). Visualized prostate volumes were divided on the basis of a sextant biopsy template into top (basal), middle, and bottom (apical) thirds on each side (38). Each sextant of the prostate gland and any metastases present were classified as positive, negative, or equivocal according to visual criteria by comparing the lesion's uptake to the background activity. Positive and equivocal findings were grouped together for statistical analysis.

For quantitative assessment, the middle slice from each sextant of the prostate was selected and used for comparative analysis of ^{18}F-FSPG PET/CT with the corresponding histologic slide (39).The maximum ^{18}F-FSPG SUVs for prostate sextants and any metastatic lesions were calculated from PET, and the bidimensional size was measured from CT. Background activity was considered as the uptake in the sextants without pathologic uptake (40). The individual readers obtained concordant SUV measurements in all subjects.

Histopathologic analysis of prostate in patients with primary prostate cancer

The analysis was carried out by board-certified surgical pathologists specializing in urologic pathology (mainly prostate), and were blinded to the imaging results. The sections were divided into six segments, that is, right (Ra) and left apex (La), right (Rm) and left middle (Lm), and right (Rb) and left base (Lb). The presence and location of cancer foci, prostatitis, and BPH were determined by the pathologist for each segment. Segments with cancer foci larger than 5 mm were defined as having prostate cancer. Other segments were classified as having normal prostate tissue, BPH, prostatitis, or BPH with prostatitis. Prostatitis and BPH were defined as follows: (i) prostatitis, dense acute and/or chronic inflammatory cell infiltration in the prostatic stroma and glands; and (ii) BPH, nodular proliferation of stromal component (early change) or both stromal and epithelial components.

Other standard imaging in patients with recurrent or metastatic prostate cancer

Investigators who were not blinded to clinical information selected up to five recurrent or metastatic lesions per patient and measured the size of each lesion on MRI, CT, or bone scan.

IHC for xCT and CD44 expression

Tissue samples obtained for routine diagnostic pathologic examination after prostatectomy were used for IHC evaluation of the xCT subunit of system x_C^- and CD44. Ten prostate samples from 8 patients were available and analyzed (in 2 patients, separate samples from the left and right lobe were available). Formalin-fixed, paraffin-embedded tissue sections were stained for xCT and CD44 using a BenchMark XT Automatic Immunostaining Device (Ventana Medical Systems) with OptiView DAB IHC Detection Kit (Ventana Medical Systems) according to the manufacturer's instructions. Four-micrometer–thick sections, obtained with a microtome, were transferred onto silanized charged slides and allowed to dry for 10 minutes at room temperature, followed by 20 minutes in an incubator at 65°C. Sections were performed by heat-induced epitope retrieval method using cell conditioning 1 buffer for 32 minutes and incubated for 16 minutes with rabbit anti-xCT (1:250 dilution; NB300-318, polyclonal anti-xCT antibody; Novus Biologicals) and mouse anti-CD44 (1:100 dilution; Clone DF 1485, monoclonal anti-CD44 antibody; DakoCytomation) in the autoimmunostainer.

The level of xCT and CD44 expression was examined by two experienced pathologists who were blinded to patient and imaging information. The results of the IHC stainings for xCT and CD44 were semiquantitatively assessed on both the proportion and intensity of the stained tumor cells. The proportion of stained tumor cells was estimated on a scale of 0–5 (0, 0%; 1, ≤1%; 2, 2%–10%; 3, 11%–33%; 4, 34%–66%; and 5, 67%–100%). The staining intensity was classified as 0 (negative), 1 (weak), 2 (moderate), or 3 (strong). The total score was calculated as the sum of the proportion score and intensity score. A total score of 3 or higher was considered as positive.

Statistical analysis

The sensitivity, specificity, and accuracy were calculated by using data collected during PET studies on a per-patient, per-lobe, and per-segment basis for primary tumors. Quantitative parameters were compared using the Mann–Whitney *U* test. The correlation of maximum ^{18}F-FSPG uptake at the 60-minute imaging timepoint (SUV_{max60}) with the intensity of xCT and CD44 IHC was assessed using Spearman rank correlation coefficients (ρ). All statistical tests were performed with SPSS Statistics (version 19; SPSS, Inc., IBM Co.) for Windows (Microsoft). $P < 0.05$ was considered to be statistically significant.

Results

The full demographics of all patients with primary prostate cancer who underwent prostatectomy after ^{18}F-FSPG PET/CT and all

Table 1. Patient characteristics.

	No.	Age (years)	PSA (ng/mL)	Gleason score	pT and pN stage	Cancer segments
Primary prostate cancer	1	66	13.0	7	pT3bpN0	Rb, Lb, Rm, Lm, Ra, La
	2	56	7.7	7	pT3apN0	Rb, Rm, Lm, Ra, La
	3	67	17.8	8	pT3apNx	Lm, Ra, La
	4	60	5.8	7	pT2cpN0	Ra
	5	68	5.8	7	pT2bpN0	Rm, Ra
	6	65	1.9	7	pT2cpN0	Lm, La
	7	77	6.6	7	pT2cpN0	Rm, Lm, Ra, La
	8	61	26.9	9	pT3bpN0	Lb, Rm, Lm, Ra, La
	9	68	9.8	8	pT2cpN0	Rm, Lm, Ra, La

	No.	Age (years)	PSA (ng/mL)	Gleason score	Sites of recurrence identified by standard imaging
Recurrent prostate cancer	1	64	8.8	7	Elevated PSA
	2	73	52.7	9	Bones
	3	68	9.9	7	Bones
	4	64	15.2	8	Bones
	5	67	3.3	7	Anterior mediastinal lymph node
	6	68	28.7	8	Bones
	7	71	71.5	8	Bones
	8	69	0.19	7	Local recurrence
	9	70	0.27	8	Right obturator lymph node
	10	75	1.2	8	Lung

enrolled patients with recurrent prostate cancer are shown in **Table 1**. ^{18}F-FSPG administration and PET imaging procedures were well tolerated. No clinically relevant changes in safety parameters were observed. Tumor samples from patients who underwent prostatectomy were staged as T2–3 adenocarcinomas by step-section histology. The cohorts with newly diagnosed and recurrent prostate cancer had a mean PSA of 9.8 and 19.2 ng/mL, respectively (range, 1.9–26.9 and 0.19–71.5 ng/mL), and a mean Gleason score of 7.5 (range, 7–9). No adverse events were reported throughout the clinical trial, either in terms of self-described symptoms, vital signs, or laboratory values.

Primary prostate cancer

PET/CT visual analysis identified abnormal ^{18}F-FSPG uptake in at least one primary prostatic tumor focus in almost all patients (8/9). PET/CT demonstrated focal ^{18}F-FSPG uptake in 15 lobes (83%) and 32 sextant segments (59%). The sensitivity, specificity, and accuracy on a lobe and sextant segment basis are listed in **Table 2**. The mean size of cancers with a negative scan was smaller than for positive scans (1.4 vs. 1.9 cm; $P = 0.036$). Overall, the detection ability was slightly higher with imaging at 105 minutes in comparison with 60 minutes. ^{18}F-FSPG PET/CT did not show extra-prostatic sites of increased uptake suggestive of metastases.

In sextants with areas of abnormal ^{18}F-FSPG uptake, the mean SUV_{max60} was 5.3 ± 2.2 and the mean tumor-to-background ratio was 2.0 ± 0.5. Comparison of ^{18}F-FSPG uptake between normal, benign, and cancerous lesions by sextant segment is shown in **Fig. 1**. The SUV_{max60} for cancer was significantly higher in comparison with both normal ($P < 0.005$) and benign pathology ($P = 0.011$), while there was no difference between normal and benign pathology ($P = 0.120$). **Figure 2** illustrates an example case with ^{18}F-FSPG PET/CT images matched to histopathologic mapping.

Recurrent prostate cancer evaluation

For recurrent prostate cancer, ^{18}F-FSPG demonstrated agreement with standard imaging in 7 of 9 patients (78%) and 13 of 18 lesions (72%) at 60 minutes, corroborating metastatic disease in the bone and lungs, as well as an anterior mediastinal node and right obturator node. In one interesting case of discordance (patient 3), a CT done just prior to the ^{18}F-FSPG PET showed sclerotic foci in the left 8th rib posteriorly, the T12 vertebra, and bilateral iliac bones. Given the recent rise in PSA, these findings were concerning for osseous metastases. ^{18}F-FSPG, however, showed intense uptake in the right apex of the prostate only ($SUV_{max60} = 6.4$; **Fig. 3**), not in any of the bone lesions, suggesting they were either benign or potentially false negative with ^{18}F-FSPG. The prostatic lesion was subsequently confirmed with a prostate MRI. The patient opted for local therapy only with radioactive seed implantation to the prostate, after which PSA dropped to undetectable levels within 3 months. Follow-up CT and MR scans for many years continued to show the bone lesions were stable, confirming their benignity and validating that the ^{18}F-FSPG PET was true negative. ^{18}F-FSPG PET also identified a focus of uptake in a patient (patient 1) presenting with elevated PSA. He had gradually rising PSA levels, but CT and bone scans were both negative. ^{18}F-FSPG PET revealed a focus of uptake ($SUV_{max60} = 3.5$) in the right apex of the prostate. Delayed imaging at 105 minutes showed one additional lesion in the left side of T2 vertebral body, which was not visualized on other imaging studies, in a patient with multifocal bone metastases.

IHC

The mean interval time between ^{18}F-FSPG PET/CT and diagnostic pathologic study was 11.1 days (range, 1–22). IHC staining of tumors revealed that all 10 primary prostate cancer samples were strongly positive for xCT (eight had a total score of 7 and two had a total score of 8). ^{18}F-FSPG uptake showed a moderate correlation with CD44

Table 2. ^{18}F-FSPG detection rates by visual analysis.

	Basis	Imaging time	Sensitivity	Specificity	Accuracy
Primary prostate cancer	Patient	60 min	89% (8/9)		
		105 min	89% (8/9)		
	Lobe	60 min	73% (11/15)	33% (1/3)	67%
		105 min	87% (13/15)	33% (1/3)	78%
	Sextant segment	60 min	53% (17/32)	73% (16/22)	61%
		105 min	63% (20/32)	68% (15/22)	65%
			Positive % agreement with standard imaging		
Recurrent prostate cancer	Patient-based		78% (7/9)		
	Lesion-based		72% (13/18)		

expression (Spearman correlation coefficient, $\rho = 0.413$; $P = 0.207$; **Fig. 4**).

Discussion

Presented herein are the first data on ^{18}F-FSPG PET/CT imaging in patients with prostate cancer. For initial diagnosis, ^{18}F-FSPG showed high tumor-to-background ratios with a relatively high tumor detection rate on both a per-patient (89%) and per-lobe (87%) basis.

The lower detection ability on a per-sextant basis may be related to the smaller size of the lesions. The smallest sized cancer that could be detected by ^{18}F-FSPG PET/CT was 6 mm, which approaches the limit of lesion detectability on clinical PET/CT systems (41). Two cancers less than 5 mm in size were not visualized.

^{18}F-FSPG PET images obtained at 105 minutes had a slightly higher sensitivity than those at 60 minutes. Baek and colleagues also reported increased tumor-to-background ratios over time up to 105 minutes in lung and breast cancers, although the tumor detection rates were the same as those obtained at 60 minutes (22). These data are consistent with the normal biodistribution and kinetics of ^{18}F-FSPG, which shows rapid clearance from the blood pool and from most organs, leading to better contrast against specific retention on the imaging timescale (20).

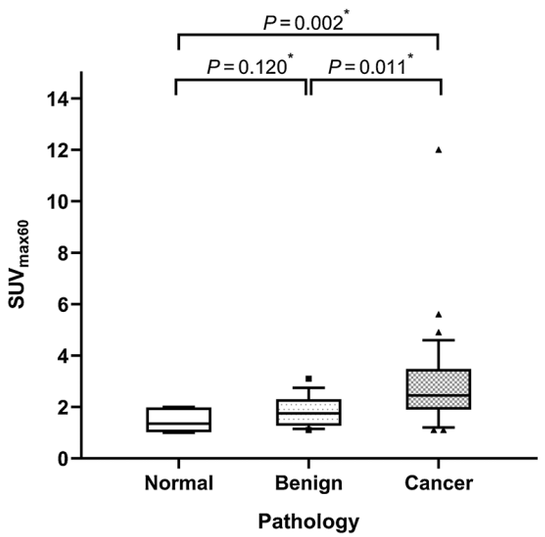

Figure 1.
Comparison of ^{18}F-FSPG uptake between normal, benign, and cancerous lesions by sextant segments in patients with primary prostate cancer. *, Mann-Whitney *U* test.

Quantitative assessment underscores the value of ^{18}F-FSPG for initial staging. The prevailing issue with the most commonly studied radiotracers in prostate cancer is that the level of accumulation can overlap in normal prostate tissue, BPH, and prostate cancer tissues, all of which often coexist (5). Inflammation also remains a challenge with tumor imaging, and high ^{18}F-FSPG uptake has been described previously in inflammatory lesions when activated macrophages or monocytes are present (34). The results of this study, however, suggest that the higher SUV_{max60} for cancer could successfully differentiate these lesions from normal tissue as well as benign pathologies including BPH and prostatitis. Very few studies in the literature on other PET radiopharmaceuticals have included benign pathologies for analysis. ^{11}C-choline and anti–^{18}F-FACBC, the only PET tracers with FDA approval for prostate cancer, showed no significant difference in uptake between cancer and benign pathologies. If the observed difference in ^{18}F-FSPG uptake between the two is reproduced in future studies with a larger number of patients, this would be the more favorable PET radiopharmaceutical to better guide targeted biopsies and minimize unnecessary ones. By visualizing a different aspect of tumor biology, the possible role of ^{18}F-FSPG in the armamentarium of molecular imaging for prostate cancer detection needs to be further elaborated in future studies. Prostate cancer is a very heterogenous disease. No one biomarker has been shown to have 100% sensitivity. For example, 42%–76% of the PSMA-PET scans were positive in the biochemical recurrence setting for those patients with PSA <2 ng/mL and 95% of the PSMA-PET scans were positive for those with > 2 ng/mL PSA, and shorter PSA doubling time increased the PSMA-PET positivity (42). Comparison with other available tracers would provide insight into the biology of imaging targets in prostate cancer.

Biochemical relapse occurs in a considerable number of patients (43). Determining the site and extent of recurrence, which have important clinical and prognostic implications, is crucial for therapeutic decision-making. ^{18}F-FSPG PET/CT demonstrated high agreement with recurrence sites identified by standard imaging. Although our gold standard was limited to standard imaging for clinical reasons, such validation appears favorable as well. It is also encouraging that while demonstrating uptake in known metastatic bone disease, suspicious findings that were later shown to be degenerative changes on follow-up were not visualized with ^{18}F-FSPG.

The significant relationship between ^{18}F-FSPG uptake and the staining intensity of the xCT subunit of system x_C^- and CD44 on IHC has been previously reported in lung and breast cancers (22). The splice variant of CD44, which is assumed to be the dominant form in

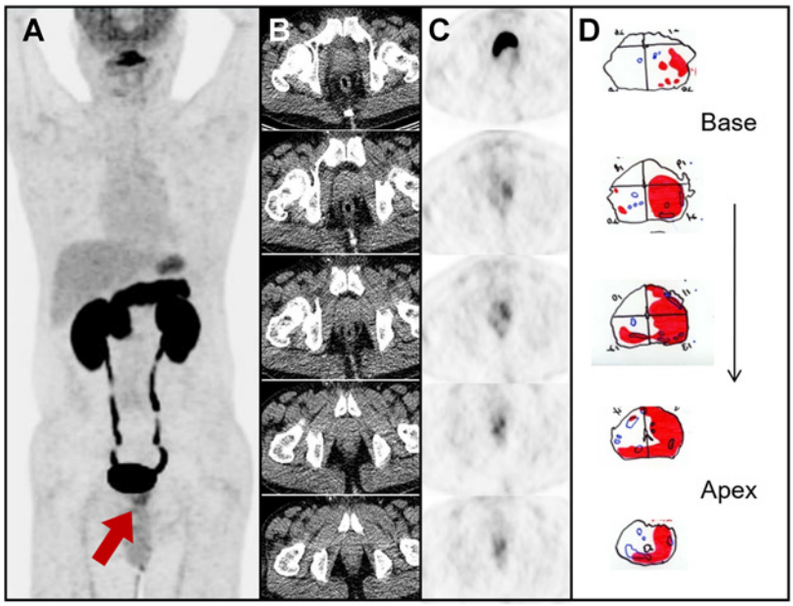

Figure 2.
A 61-year-old male with primary prostate cancer. **A,** Maximum intensity projection of ^{18}F-FSPG PET showed increased uptake in the prostate. Focal uptakes in the bilateral prostate lobes on the serial transaxial CT and ^{18}F-FSPG PET images (**B** and **C**) were matched with the areas of cancer, in red, in the corresponding histopathologic maps of the prostate (**D**).

tumors, supports balancing the redox status in cancer cells by stabilizing the xCT light chain subunit of system x_C^-. The light chain subunit confers transport function, mediating uptake of ^{18}F-FSPG and cystine, the latter of which is used for glutathione biosynthesis. It was shown in a previous study that tumors with strong expression of both xCT and CD44 showed high ^{18}F-FSPG uptake, while the absence of either resulted in low uptake (22). Similarly, we found a moderate correlation between SUV_{max60} and CD44 expression. High-level expression of CD44 has also been causally linked to progression, with studies supporting the definitive role of CD44 in prostate tumor growth and metastasis (44). All of our patients expressed xCT strongly with scores 7–8, so it was difficult to draw any conclusions. However, given the mutual dependence of the two markers for correlation with ^{18}F-FSPG uptake, it is worth emphasizing that in the context of positive xCT, CD44 demonstrated a relationship with ^{18}F-FSPG, possibly by stabilizing the xCT subunit (45).

As a study of exploratory nature, the number of patients included in each cohort was small, limiting its statistical power. In particular, the redundancy in xCT scores precluded multivariate analysis with various combinations of the two IHC markers. Also, considering the potential tumor heterogeneity in terms of xCT and CD44 expression as well as ^{18}F-FSPG uptake, a more rigorous slice-by-slice comparison would provide more information on the complex biology of prostate cancer and a better understanding of chemoresistance mechanisms.

Conclusion

^{18}F-FSPG is a promising tumor-imaging agent for PET that seems to have favorable biodistribution and high cancer detection rate in patients with prostate cancer. ^{18}F-FSPG PET/CT was able to successfully differentiate cancerous prostate lesions from normal tissue as well as benign pathologies such as BPH. Further studies are warranted to determine the diagnostic value in both the initial staging and

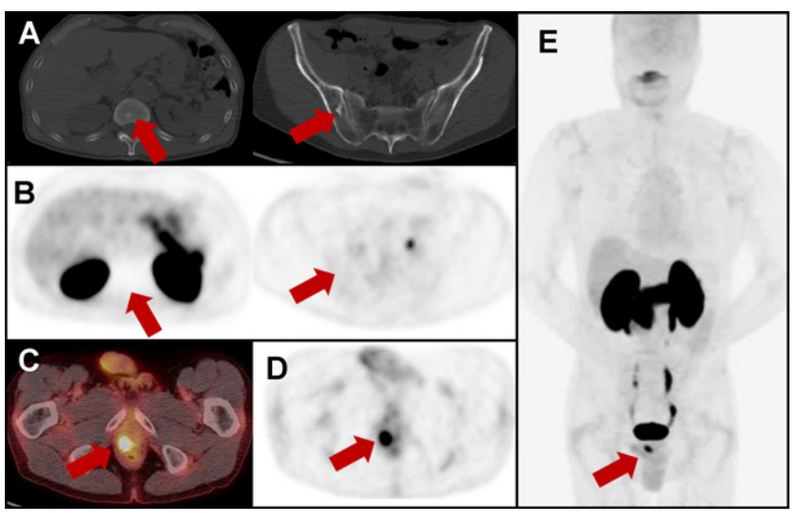

Figure 3.
A 68-year-old male with recurrent prostate cancer. Sclerotic lesions in the T12 vertebral body and the right iliac bone on the CT images (**A**) showed no ^{18}F-FSPG uptake on the PET images (**B**). Focal uptake was noted in the right side of the prostate lobe on the fused ^{18}F-FSPG PET/CT (**C**), ^{18}F-FSPG PET (**D**), and maximum intensity projection (**E**) images. This prostatic lesion was subsequently confirmed with a prostate MRI. Following local radiation treatment to the prostate, the PSA became undetectable. Follow-up CT and MR scans for many years continued to show the bone lesions were stable, confirming their benignity and validating that the ^{18}F-FSPG PET was true negative.

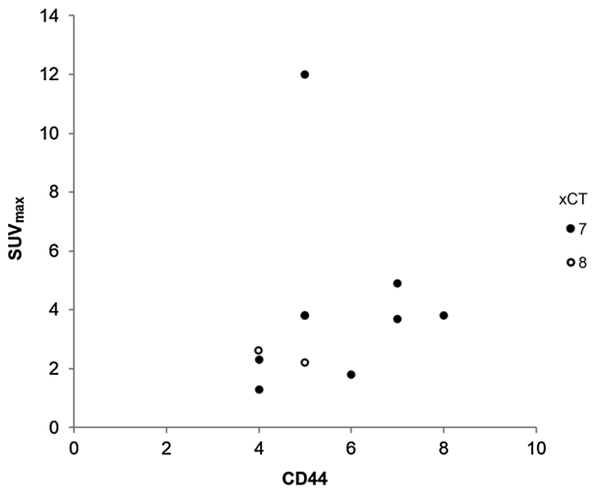

Figure 4.
Scatterplot of ^{18}F-FSPG uptake and CD44 expression. The total score for xCT staining was either 7 (filled circles) or 8 (open circles). Spearman correlation coefficient was calculated ($\rho = 0.413$; $P = 0.207$), but one unexplained outlier with very high ^{18}F-FSPG uptake ($SUV_{max60} = 12$) was not included in the correlation analysis.

recurrence settings, and how it compares with other investigational/approved radiotracers as well as other conventional imaging modalities.

Disclosure of Potential Conflicts of Interest

N. Koglin reports personal fees from Life Molecular Imaging GmbH (employment) during the conduct of the study, and is listed as a coinventor on a patent application on "[F-18]-labeled L-glutamic acid and L-glutamine derivatives (I), their use and processes for their preparation; US 9,308,282" that is owned by Life Molecular Imaging. S. Bullich reports personal fees from Life Molecular Institution (employment) during the conduct of the study. A. Mueller reports personal fees from Life Molecular Imaging GmbH (employment) during the conduct of the study, and is listed as a coinventor on a patent application on "[F-18]-labeled L-glutamic acid and L-glutamine derivatives (I), their use and processes for their preparation; US 9,308,282" that is owned by Life Molecular Imaging. M. Berndt reports personal fees from Life Molecular Imaging (employment) during the conduct of the study, and is listed as a coinventor on a patent application on "precursors of glutamate derivatives, US 9,000,037" that is owned by Life Molecular Imaging and "[F-18]-labeled L-glutamic acid and L-glutamine derivatives (I), their use and processes for their preparation; US 9,308,282" that is owned by Life Molecular Imaging. A.W. Stephens reports personal fees from Life Molecular Imaging GmbH (employment) during the conduct of the study, and is listed as a coinventor on a patent application on "[F-18]-labeled L-glutamic acid and L-glutamine derivatives (I), their use and processes for their preparation; US 9,308,282" that is owned by Life Molecular Imaging. D.H. Moon reports grants from Life Molecular Imaging GmbH (Piramal Imaging GmbH) during the conduct of the study; grants from GE Healthcare (myocardial perfusion study in patients with stable coronary artery disease), Taiho Pharmaceutical (FLT PET imaging study), and Life Molecular Imaging GmbH (formerly Piramal Imaging GmbH, F-18 FSPG clinical trial for imaging inflammation and F-18 GP1 clinical trial for imaging thrombosis) outside the submitted work; and is listed as a coinventor on a provisional patent application on fluorination of radiopharmaceuticals that is owned by Asan Foundation (Asan Medical Center). S.S. Gambhir reports personal fees from AbbVie (consulting), other income and/or support from Akrotome Imaging (stock), CellSight Technologies (stock, founder, spouse is CEO), Click Diagnostics (stock), CytomX Therapeutics (stock), ImaginAb (stock), Life Molecular Imaging (consulting), MagArray (stock), NinePoint Medical (stock), Nodus Therapeutics (stock), PureTech (scientific advisory board, stock), RefleXion (scientific advisory board, stock), SiteOne Therapeutics (scientific advisory board, stock), and Spectrum Dynamics (stock), and personal fees and other from Taumark (medical and scientific advisory board), Earli (founder, board member, stock), Endra (cofounder, board member, stock), Grail (stock, scientific advisory board), Nines (scientific advisory board, stock), Nusano (stock), and Vave Health (scientific advisory board, stock) outside the submitted work. E.S. Mittra reports grants and personal fees from Advanced Accelerator Applications (clinical trial and consulting) and ImaginAb (clinical trial and consulting) outside the submitted work. No potential conflicts of interest were disclosed by the other authors.

Authors' Contributions

S.Y. Park: Resources, formal analysis, validation, writing-original draft, writing-review and editing. **S.J. Na:** Conceptualization, data curation, investigation, writing-review and editing. **M. Kumar:** Data curation, investigation, writing-review and editing. **C. Mosci:** Data curation, investigation, writing-review and editing. **M. Wardak:** Writing-review and editing. **N. Koglin:** Conceptualization, resources, formal analysis, methodology, writing-review and editing. **S. Bullich:** Resources, formal analysis, methodology, writing-review and editing. **A. Mueller:** Resources, formal analysis, methodology, writing-review and editing. **M. Berndt:** Resources, formal analysis, methodology, writing-review and editing. **A.W. Stephens:** Resources, formal analysis, methodology, writing-review and editing. **Y.M. Cho:** Data curation, validation, investigation, writing-review and editing. **H. Ahn:** Data curation, investigation, methodology, writing-review and editing. **S.Y. Chae:** Data curation, validation, writing-review and editing. **H.O. Kim:** Data curation, validation, investigation, writing-review and editing. **D.H. Moon:** Conceptualization, validation, investigation, writing-review and editing. **S.S. Gambhir:** Conceptualization, resources, supervision, funding acquisition, methodology, writing-review and editing. **E.S. Mittra:** Conceptualization, data curation, supervision, funding acquisition, validation, methodology, writing-review and editing.

Acknowledgments

The clinical work was supported by funding from Bayer HealthCare, Inc. as part of a sponsored clinical research trial. We would like to thank the research study participants and their families, our referring physicians, our clinical research coordinators, and the Radiochemistry Facility and staff, in particular Dr. Frederick T. Chen, Dr. Bin Shen, Amit Hetstron, and So-Hee Kim. We further appreciate the assistance of Lüder M. Fels, Claudia Bacher-Stier, and our PET/CT technologists. We are grateful for the funding support provided by the Ben and Catherine Ivy Foundation (to S.S. Gambhir) and the NCI In Vivo Cellular & Molecular Imaging Center grant (ICMIC P50 to S.S. Gambhir). The authors dedicate this paper to the memory of our beloved mentor, colleague, and friend, Dr. Sanjiv Sam Gambhir, who passed away shortly after the acceptance of this manuscript. He was instrumental to this project and will be dearly missed. We keep him in our hearts and will carry on his legacy.

The costs of publication of this article were defrayed in part by the payment of page charges. This article must therefore be hereby marked *advertisement* in accordance with 18 U.S.C. Section 1734 solely to indicate this fact.

Received February 18, 2020; revised May 25, 2020; accepted July 14, 2020; published first July 21, 2020.

References

1. Bray F, Ferlay J, Soerjomataram I, Siegel RL, Torre LA, Jemal A. Global cancer statistics 2018: GLOBOCAN estimates of incidence and mortality worldwide for 36 cancers in 185 countries. CA Cancer J Clin 2018;68:394–424.
2. Xu J, Murphy SL, Kochanek KD, Bastian BA. Deaths: final data for 2013. Natl Vital Stat Rep 2016;64:1–119.
3. Liesenfeld L, Kron M, Gschwend JE, Herkommer K. Prognostic factors for biochemical recurrence more than 10 years after radical prostatectomy. J Urol 2017;197:143–8.
4. Bjurlin MA, Rosenkrantz AB, Beltran LS, Raad RA, Taneja SS. Imaging and evaluation of patients with high-risk prostate cancer. Nat Rev Urol 2015;12:617–28.
5. Wallitt KL, Khan SR, Dubash S, Tam HH, Khan S, Barwick TD. Clinical PET imaging in prostate cancer. Radiographics 2017;37:1512–36.
6. Woodrum DA, Kawashima A, Gorny KR, Mynderse LA. Prostate cancer: state of the art imaging and focal treatment. Clin Radiol 2017;72:665–79.
7. Treglia G, Ceriani L, Sadeghi R, Giovacchini G, Giovanella L. Relationship between prostate-specific antigen kinetics and detection rate of radiolabelled

choline PET/CT in restaging prostate cancer patients: a meta-analysis. Clin Chem Lab Med 2014;52:725–33.
8. Jadvar H. Molecular imaging of prostate cancer with PET. J Nucl Med 2013;54: 1685–8.
9. Lütje S, Heskamp S, Cornelissen AS, Poeppel TD, van den Broek SA, Rosenbaum-Krumme S, et al. PSMA ligands for radionuclide imaging and therapy of prostate cancer: clinical status. Theranostics 2015;5:1388–401.
10. Sarkar S, Das S. A review of imaging methods for prostate cancer detection. Biomed Eng Comput Biol 2016;7:1–15.
11. Jadvar H. Positron emission tomography in prostate cancer: summary of systematic reviews and meta-analysis. Tomography 2015;1:18–22.
12. Banerjee SR, Pomper MG. Clinical applications of Gallium-68. Appl Radiat Isot 2013;76:2–13.
13. Minamimoto R, Hancock S, Schneider B, Chin FT, Jamali M, Loening A, et al. Pilot comparison of ^{68}Ga-RM2 PET and ^{68}Ga-PSMA-11 PET in patients with biochemically recurrent prostate cancer. J Nucl Med 2016;57:557–62.
14. Werner RA, Derlin T, Lapa C, Sheikbahaei S, Higuchi T, Giesel FL, et al. ^{18}F-Labeled, PSMA-targeted radiotracers: leveraging the advantages of radiofluorination for prostate cancer molecular imaging. Theranostics 2020;10:1–16.
15. Zhang-Yin J, Provost C, Cancel-Tassin G, Rusu T, Penent M, Radulescu C, et al. A comparative study of peptide-based imaging agents [^{68}Ga]Ga-PSMA-11, [^{68}Ga]Ga-AMBA, [^{68}Ga]Ga-NODAGA-RGD and [^{68}Ga]Ga-DOTA-NT-20.3 in preclinical prostate tumour models. Nucl Med Biol 2020;84–85:88–95.
16. Koglin N, Mueller A, Berndt M, Schmitt-Willich H, Toschi L, Stephens AW, et al. Specific PET imaging of xC- transporter activity using a ^{18}F-labeled glutamate derivative reveals a dominant pathway in tumor metabolism. Clin Cancer Res 2011;17:6000–11.
17. Beinat C, Gowrishankar G, Shen B, Alam IS, Robinson E, Haywood T, et al. The characterization of ^{18}F-hGTS13 for molecular imaging of xC (-) transporter activity with PET. J Nucl Med 2019;60:1812–7.
18. Webster JM, Morton CA, Johnson BF, Yang H, Rishel MJ, Lee BD, et al. Functional imaging of oxidative stress with a novel PET imaging agent, ^{18}F-5-fluoro-L-aminosuberic acid. J Nucl Med 2014;55:657–64.
19. Yang H, Jenni S, Colovic M, Merkens H, Poleschuk C, Rodrigo I, et al. ^{18}F-5-fluoroaminosuberic acid as a potential tracer to gauge oxidative stress in breast cancer models. J Nucl Med 2017;58:367–73.
20. Mosci C, Kumar M, Smolarz K, Koglin N, Stephens AW, Schwaiger M, et al. Characterization of physiologic ^{18}F-FSPG uptake in healthy volunteers. Radiology 2016;279:898–905.
21. Smolarz K, Krause BJ, Graner FP, Wagner FM, Hultsch C, Bacher-Stier C, et al. (S)-4-(3–^{18}F-fluoropropyl)-L-glutamic acid: an ^{18}F-labeled tumor-specific probe for PET/CT imaging–dosimetry. J Nucl Med 2013;54:861–6.
22. Baek S, Choi CM, Ahn SH, Lee JW, Gong G, Ryu JS, et al. Exploratory clinical trial of (4S)-4-(3-[^{18}F]fluoropropyl)-L-glutamate for imaging xC- transporter using positron emission tomography in patients with non-small cell lung or breast cancer. Clin Cancer Res 2012;18:5427–37.
23. Baek S, Mueller A, Lim YS, Lee HC, Lee YJ, Gong G, et al. (4S)-4-(3-^{18}F-fluoropropyl)-L-glutamate for imaging of xC transporter activity in hepatocellular carcinoma using PET: preclinical and exploratory clinical studies. J Nucl Med 2013;54:117–23.
24. Cheng MF, Huang YY, Ho BY, Kuo TC, Hsin LW, Shiue CY, et al. Prospective comparison of (4S)-4-(3-^{18}F-fluoropropyl)-L-glutamate versus ^{18}F-fluorodeoxyglucose PET/CT for detecting metastases from pancreatic ductal adenocarcinoma: a proof-of-concept study. Eur J Nucl Med Mol Imaging 2019;46:810–20.
25. Kavanaugh G, Williams J, Morris AS, Nickels ML, Walker R, Koglin N, et al. Utility of [^{18}F]FSPG PET to image hepatocellular carcinoma: first clinical evaluation in a U.S. population. Mol Imaging Biol 2016;18:924–34.
26. Mittra ES, Koglin N, Mosci C, Kumar M, Hoehne A, Keu KV, et al. Pilot preclinical and clinical evaluation of (4S)-4-(3-[^{18}F]Fluoropropyl)-L-glutamate (^{18}F-FSPG) for PET/CT imaging of intracranial malignancies. PLoS One 2016; 11:e0148628.
27. Magarik MA, Walker RC, Gilbert J, Manning HC, Massion PP. Intracardiac metastases detected by ^{18}F-FSPG PET/CT. Clin Nucl Med 2018;43:28–30.
28. Arensman MD, Yang XS, Leahy DM, Toral-Barza L, Mileski M, Rosfjord EC, et al. Cystine-glutamate antiporter xCT deficiency suppresses tumor growth while preserving antitumor immunity. Proc Natl Acad Sci U S A 2019;116: 9533–42.
29. Lewerenz J, Hewett SJ, Huang Y, Lambros M, Gout PW, Kalivas PW, et al. The cystine/glutamate antiporter system x(c)(-) in health and disease: from molecular mechanisms to novel therapeutic opportunities. Antioxid Redox Signal 2013;18:522–55.
30. Lim JKM, Delaidelli A, Minaker SW, Zhang HF, Colovic M, Yang H, et al. Cystine/glutamate antiporter xCT (SLC7A11) facilitates oncogenic RAS transformation by preserving intracellular redox balance. Proc Natl Acad Sci U S A 2019;116:9433–42.
31. Nagano O, Okazaki S, Saya H. Redox regulation in stem-like cancer cells by CD44 variant isoforms. Oncogene 2013;32:5191–8.
32. Greenwood HE, McCormick PN, Gendron T, Glaser M, Pereira R, Maddocks ODK, et al. Measurement of tumor antioxidant capacity and prediction of chemotherapy resistance in preclinical models of ovarian cancer by positron emission tomography. Clin Cancer Res 2019;25:2471–82.
33. McCormick PN, Greenwood HE, Glaser M, Maddocks ODK, Gendron T, Sander K, et al. Assessment of tumor redox status through (S)-4-(3-[^{18}F]fluoropropyl)-L-glutamic acid PET imaging of system xc(-) activity. Cancer Res 2019;79: 853–63.
34. Chae SY, Choi CM, Shim TS, Park Y, Park CS, Lee HS, et al. Exploratory clinical investigation of (4S)-4-(3-^{18}F-Fluoropropyl)-l-glutamate PET of inflammatory and infectious lesions. J Nucl Med 2016;57:67–9.
35. Hoehne A, James ML, Alam IS, Ronald JA, Schneider B, D'Souza A, et al. [^{18}F]FSPG-PET reveals increased cystine/glutamate antiporter (xc-) activity in a mouse model of multiple sclerosis. J Neuroinflammation 2018;15:55.
36. Zhong W, Weiss HL, Jayswal RD, Hensley PJ, Downes LM, St Clair DK, et al. Extracellular redox state shift: a novel approach to target prostate cancer invasion. Free Radic Biol Med 2018;117:99–109.
37. Kwee SA, Thibault GP, Stack RS, Coel MN, Furusato B, Sesterhenn IA. Use of step-section histopathology to evaluate ^{18}F-fluorocholine PET sextant localization of prostate cancer. Mol Imaging 2008;7:12–20.
38. Kwee SA, Wei H, Sesterhenn I, Yun D, Coel MN. Localization of primary prostate cancer with dual-phase ^{18}F-fluorocholine PET. J Nucl Med 2006;47:262–9.
39. Reske SN, Blumstein NM, Neumaier B, Gottfried HW, Finsterbusch F, Kocot D, et al. Imaging prostate cancer with ^{11}C-choline PET/CT. J Nucl Med 2006;47: 1249–54.
40. Farsad M, Schiavina R, Castellucci P, Nanni C, Corti B, Martorana G, et al. Detection and localization of prostate cancer: correlation of ^{11}C-choline PET/CT with histopathologic step-section analysis. J Nucl Med 2005;46:1642–9.
41. Adler S, Seidel J, Choyke P, Knopp MV, Binzel K, Zhang J, et al. Minimum lesion detectability as a measure of PET system performance. EJNMMI Phys 2017;4:13.
42. Perera M, Papa N, Christidis D, Wetherell D, Hofman MS, Murphy DG, et al. Sensitivity, specificity, and predictors of positive ^{68}Ga-Prostate-specific membrane antigen positron emission tomography in advanced prostate cancer: a systematic review and meta-analysis. Eur Urol 2016;70:926–37.
43. Mohler JL, Kantoff PW, Armstrong AJ, Bahnson RR, Cohen M, D'Amico AV, et al. Prostate cancer, version 2.2014. J Natl Compr Canc Netw 2014;12:686–718.
44. Lokeshwar BL, Lokeshwar VB, Block NL. Expression of CD44 in prostate cancer cells: association with cell proliferation and invasive potential. Anticancer Res 1995;15:1191–8.
45. Ishimoto T, Nagano O, Yae T, Tamada M, Motohara T, Oshima H, et al. CD44 variant regulates redox status in cancer cells by stabilizing the xCT subunit of system xc(-) and thereby promotes tumor growth. Cancer Cell 2011;19:387–400.